



# Clock systematic jump estimation and URA refinement of BDS-3 B2b real-time precise point positioning service

Junping Chen<sup>1,2</sup> · Ziyuan Song<sup>1,3</sup> · Yize Zhang<sup>1,2</sup> · Junsheng Ding<sup>4</sup> · Xin Jiang<sup>3</sup> · Sainan Yang<sup>3</sup> · Yangfei Hou<sup>3</sup>

Received: 5 November 2024 / Accepted: 17 February 2025  
© The Author(s), under exclusive licence to Springer-Verlag GmbH Germany, part of Springer Nature 2025

## Abstract

The real-time precise point positioning (RT-PPP) service of BDS-3 (PPP-B2b) was launched in July 2021 to deliver a decimeter-level positioning service for users in China and its surrounding areas. During the use of PPP-B2b, we identified two issues adversely affecting positioning performance: systematic jumps in GPS clock bias and inaccuracies of the URA parameter. This paper analyzes the impact of these issues on PPP performance and proposes practical solutions. To address the GPS clock bias, we introduce three user-side strategies, including a jump detection and clock splicing method combined with various inter-system bias (ISB) estimation strategies. Performance comparisons reveal that effective bias processing can reduce the three-dimensional root-mean-square error (RMSE) from 0.83 to 0.08 m in kinematic mode. Additionally, we validate the insufficient accuracy of broadcasted URA and propose an approach to re-estimate the phase URA using data from over 50 monitoring stations across China, demonstrating that the refined URA enhances the PPP-B2b positioning stochastic model and this provides a viable direction for optimizing the PPP-B2b service.

**Keywords** BDS-3 · PPP-B2b · GPS clock jump bias · URA

## Introduction

Significant progress has been made in precise point positioning (PPP) over the last two decades, owing to its high precision and ease of operation (Malys and Jensen 1900; Kouba et al. 2001; Odijk et al. 2016; Geng et al. 2024). Real-time PPP (RT-PPP) has garnered increased attention from scholars since 2013 (Chen et al. 2013), coinciding with the official launch of the real-time service (RTS) by the International GNSS Service (IGS). RT-PPP relies on broadcast ephemeris, real-time orbit, clock corrections, and other corrections provided to users (IGS 2020), which are formatted into state space representation (SSR) messages and transmitted via the

standard of the radio technical commission for maritime services (RTCM) (RTCM, 2016) using the Networked Transport of RTCM via Internet Protocol (NTRIP) (Weber et al. 2007). Since its inception, RT-PPP has been widely utilized and demonstrated decimeter to centimeter-level accuracy (Shi et al. 2017; Wang et al. 2022).

To overcome reliance on the internet and provide continuous RT-PPP, many commercial companies have developed satellite communication links to offer RT-PPP services, such as RTX by Trimble (Leandro, 2011), OmniStar (Booth and Snow 2009), and NavCom (Dai et al. 2016). However, the high subscription costs of satellite-based services may be prohibitive for individual users. With the ongoing development of augmentation services, many navigation satellite systems have integrated high-accuracy services into their signals. For example, the new multi-GNSS advanced orbit and clock augmentation precise point positioning service (MODOCA-PPP) of QZSS launched experimental service on September 30, 2022, aiming for full service in 2024 (Cabinet Office, 2022). Galileo's high accuracy service (HAS) initiated its initial PPP service embedded on the E6-B signal on January 24, 2023, targeting 95% accuracy of 0.2 m and 0.4 m for horizontal and vertical positioning globally (European GNSS Service Center, 2023; Fernandez-Hernandez et al. 2022). The BDS navigation satellite system has also

✉ Junping Chen  
junping@shao.ac.cn

<sup>1</sup> Shanghai Astronomical Observatory, Chinese Academy of Sciences, Shanghai 200030, China  
<sup>2</sup> University of Chinese Academy of Sciences, Beijing 100049, China  
<sup>3</sup> China Mobile (Shanghai) Information and Communication Technology Co., Ltd, Shanghai 200120, China  
<sup>4</sup> Department of Land Surveying and Geo-Informatics, The Hong Kong Polytechnic University, Hong Kong 999077, China

begun providing enhanced positioning services since the completion of the BDS-2 regional service, offering decimeter-level accuracy for users in China and surrounding areas (Zhang et al. 2019; Wang et al. 2020; Chen et al. 2022a). However, the positioning augmentation message of BDS is currently only available for authorized users (Chen et al. 2020). Fortunately, with the official launch of the BDS-3 global navigation satellite system, BDS has improved the performance of positioning and global short message services globally (Chen et al. 2022b; Song et al. 2023). Besides, the open RT-PPP service has been announced as available since July 2021. The corrections are embedded in the BDS-3 B2b signal, broadcasted by BDS-3 GEO satellites. The broadcasted correction parameters in the BDS-3 PPP-B2b service include satellite precise orbit and clock offset parameters of BDS-3 and other Global Navigation Satellite Systems (GNSS), and provides PPP services for users in China and its surrounding areas (CSNO, 2020).

Numerous scholars have focused on BDS-3 PPP-B2b products and positioning performance. Xu et al. (2021) evaluated the orbit and clock precision of PPP-B2b. The MEO orbit accuracy reached 6.8 cm, 33.4 cm, and 36.6 cm in the radial, along-track, and cross-track directions, respectively, and the standard deviation of PPP-B2b clock offset was approximately 0.12 ns. Jun et al. (2021) assessed BDS-3 PPP-B2b RTS compared to CNES RTS and demonstrated the comparability of the PPP-B2b service to CNES RTS. Sun et al. (2023) confirmed the long-term stability of the B2b PPP service. Geng et al. (2022) implemented kinematic PPP-B2b on a marine vehicle and evaluated its positioning accuracy. Wu et al. (2023) further verified the PPP-B2b performance on other platforms, including offshore vessels and unmanned aircraft. Xu et al. (2023) proposed an improved method of B2b PPP by estimating signal in space range errors (SISRE) and demonstrated its validity. In the research by He et al. (2023), the jump bias of GPS clock correction in PPP-B2b service was proposed for the first time. They set the inter-system bias (ISB) as a white noise (WN) parameter to eliminate its impact on positioning and emphasized the unsuitability of setting the ISB parameter as a constant value when performing GPS + BDS-3 PPP-B2b due to the jump bias. However, the effect of the systematic bias on PPP-B2b has not been thoroughly analyzed, and effective strategies to address the jump bias require further

study. Additionally, the user range accuracy index (URAI) is broadcasted along with the orbit correction in the PPP-B2b service, yet it has not garnered attention from scholars. Given the effectiveness of URAI in observation weighting (Wang, 2019), evaluating the broadcasted B2b URA series and its performance applied to the observation stochastic model is worthwhile.

In this paper, we represent the PPP-B2b positioning model along with its stochastic model at first. Then, the systematic jump bias of GPS clock and its adverse effects on BDS/GPS dual-system positioning is analyzed. To mitigate this bias, we propose a jump bias detection and splicing method, combining it with different ISB estimation methods. Beyond that, we utilize the URA for PPP-B2b and reveal its poor accuracy in PPP. Therefore, we propose a phase-based URA refining strategy and prove its effectiveness in improve user positioning performance.

## Methodology

### PPP-B2b corrections usage and positioning model

The real-time corrections in PPP-B2b service consist of four message types, including satellite mask, orbit correction and, user range error index (URAI), clock offset correction and differential code bias (DCB) correction. The specific messages for each type are outlined in Table 1.

To ensure accurate matching of B2b PPP corrections with the broadcast ephemeris, the issue of data (IOD) in the SSR messages of all types must initially be consistent. Subsequently, the IODN broadcasted in Type 2 messages is utilized to match the IODE in the broadcast ephemeris. It's important to note that the B2b corrections for BDS-3 are applied to the CNAV1 navigation message, while the corrections for GPS are applied to the LNAV navigation message. The precise satellite coordinate  $X_{prec}^s$  calculated using B2b orbit corrections can be expressed as:

$$X_{prec}^s = X_{brd}^s - \delta X^s \quad (1)$$

where  $X_{brd}^s$  represents the coordinate calculated using broadcast ephemeris and  $\delta X^s$  denotes the orbit corrections in the earth-center-earth-fixed (ECEF) frame.

**Table 1** Four types of the B2b PPP service messages

Type No	Message	System	Broadcast frequency (s)	Correction validity time (s)
Type 1	Satellite mask	GPS + BDS-3	48	/
Type 2	Satellite orbit correction and URAI	GPS + BDS-3	48	96
Type 3	Satellite DCB	BDS-3	48	86,400
Type 4	Satellite clock correction	GPS + BDS-3	6	12

The B2b orbit corrections are broadcasted in satellite coordinate system. The conversion formula from the satellite coordinate system to the earth-centered earth-fixed (ECEF) frame for B2b orbit corrections is as follows:

$$\delta X^s = [e_r, e_a, e_c] \cdot \delta^s \tag{2}$$

with

$$\begin{cases} e_a = e_c \times e_r \\ e_c = \frac{r \times \dot{r}}{|r \times \dot{r}|} \\ e_r = \frac{\dot{r}}{|\dot{r}|} \end{cases} \tag{3}$$

where  $r$  and  $\dot{r}$  represent the position and velocity vectors of the satellites in the ECEF frame, which can be calculated using the broadcast ephemeris.  $\delta^s$  represents the orbit correction broadcasted by PPP-B2b.

The URAI calculation formula is:

$$URA \leq 3^{I_{class}} (1 + 0.25 * I_{value}) - 1 \tag{4}$$

where the parameter range accuracy class ( $I_{class}$ ) and user range accuracy value ( $I_{value}$ ) are broadcasted along with the orbit corrections in Type 2.

To align the B2b clock corrections, the determination of the Satellite PRN in type 4 relies on the Sat Slot parameter and the satellite mask broadcasted in Type 1. Additionally, the ‘‘IOD Corr’’ parameter (IODE of the corrections) broadcasted in type 4 (CSNO, 2020) for each satellite must be consistent with the same parameter in Type 2 for broadcast ephemeris matching. The B2b precise clock offset  $C_{prec}^s$  can be expressed as:

$$C_{prec}^s = C_{BRD} - \frac{\delta C_0}{c} \tag{5}$$

where  $C_{BRD}$  represents the satellite clock offset calculated from broadcast ephemeris;  $\delta C_0$  denotes the B2b clock corrections and  $c$  represents the light speed.

In this paper, the PPP model with ionosphere free (IF) combination is adopted and the observation equation is written as:

$$\begin{cases} P_{IF,r}^s = \rho_r^s + c \cdot (dt_{r,IF} - dt_{IF}^s) + M_r^s d_{trop,r} + (B_{IF,r} - B_{IF}^s) + \varepsilon(P_{IF,r}^s) \\ \Phi_{IF,r}^s = \rho_r^s + c \cdot (dt_{r,IF} - dt_{IF}^s) + M_r^s d_{trop,r} + (b_{IF,r} - b_{IF}^s) + N_{IF}^s + \varepsilon(\Phi_{IF,r}^s) \end{cases} \frac{n!}{r!(n-r)!} \tag{6}$$

where  $P_{IF,r}^s$  and  $\Phi_{IF,r}^s$  denote the IF combination of the pseudorange and carrier phase observations, respectively;  $\rho_r^s$  represents the geometrical propagation distances between satellite and receiver,  $dt_{r,IF}$  and  $dt_{IF}^s$  denote the receiver and satellite clock error in IF combination, respectively; Note that the satellite coordinate while calculating  $\rho_r^s$  and

the satellite clock error  $dt_{IF}^s$  has been corrected using the B2b orbit and clock corrections.  $d_{trop,r}$  and  $M_r^s$  represent the zenith tropospheric delay and its mapping function, respectively;  $B_{IF,r}$  and  $B_{IF}^s$  denote the code bias for the receiver and satellite, respectively; and  $b_{IF,r}$  and  $b_{IF}^s$  represent the phase bias for the receiver and satellites, respectively.  $N_{IF}^s$  and  $\lambda_{IF}$  denote the IF phase ambiguity and its wavelength, respectively.  $\varepsilon(P_{IF,r}^s)$  and  $\varepsilon(\Phi_{IF,r}^s)$  represent the noise of the IF combination for pseudorange and carrier phase observations, respectively. Considering the parameter reorganization, formula (6) can be further expressed as:

$$\begin{cases} P_{IF,r}^s = \rho_r^s + c \cdot (\overline{dt}_{r,IF} - \overline{dt}_{IF}^s) + M_r^s d_{trop,r} + \varepsilon(P_{IF,r}^s) \\ \Phi_{IF,r}^s = \rho_r^s + c \cdot (\overline{dt}_{r,IF} - \overline{dt}_{IF}^s) + M_r^s d_{trop,r} + \overline{N}_{IF}^s + \varepsilon(\Phi_{IF,r}^s) \end{cases} \tag{7}$$

where  $\overline{dt}_{r,IF} = dt_{r,IF} + B_{IF,r}$ ,  $\overline{dt}_{IF}^s = dt_{IF}^s + B_{IF}^s$ ,  $\overline{N}_{IF}^s = \lambda_{IF} N_{IF}^s + b_{IF,r} - b_{IF}^s - B_{IF,r} + B_{IF}^s$ .

Considering the dual-system positioning, the estimated-vector  $dx$  can be expressed as:

$$dx = [\Delta r, \overline{dt}_{r,IF}, d_{trop,r}, \overline{N}_{IF}^s, d_{ISB}] \tag{8}$$

where  $d_{ISB}$  represents the inter-system bias between GPS and BDS-3.

Since the datum of BDS-3 clock is based on B3I while the time group delays (TGDs) in CNAV1 are corrected for B1C and B2a, the DCB corrections in Type 3 need to be used for B1I/B3I PPP.

According to the positioning model, its stochastic model can be expressed as:

$$\sigma^{s2} = \sigma_{noise}^s{}^2 + \sigma_{orb}^2 + \sigma_{clk}^2 + \sigma_{Trop}^2 + \sigma_{ION}^2 \tag{9}$$

where  $\sigma_{orb}$ ,  $\sigma_{clk}$ ,  $\sigma_{Trop}$  and  $\sigma_{ION}$  denote the orbit error, clock error, tropospheric error and ionospheric error, respectively. When the broadcasted URA are not considered,  $\sigma_{orb}$  and  $\sigma_{clk}$  are unknown, along with estimating the troposphere and using the IF combination to eliminate the first order of the ionospheric delay, all four parameters mentioned above are

initially set to 0 by default.  $\sigma_{noise}^s$  represents the observation noise with satellite elevation angle factor, which can be expressed as:

$$\sigma_{noise}^s = \sigma_{Obs} * \varphi = \sigma_{Obs} * \left( 0.5 + \frac{0.5}{\sin(A_{Ele})} \right) \quad (10)$$

where  $\sigma_{noise}^s$  represents the weight of satellite  $s$ .  $\sigma_{Obs}$  denotes the observation noise, usually set as 0.3 m for origin pseudorange observations and 0.003 m for origin carrier phase observations, respectively. When using IF combination, it enlarges 3 times.  $A_{Ele}$  represents the satellite elevation angle.

URA is typically derived from multiple monitoring stations on the server end through statistical calculations of pseudorange or phase residuals. Its value comprehensively reflects the accuracy of satellite orbit and clock errors (Wang et al., 2013). Therefore, we incorporate the broadcasted B2B URA into the stochastic model,  $\sigma^s$  can be expressed as:

$$\sigma^{s2} = \sigma_{noise}^{s2} + \sigma_{URA}^{s2} \quad (11)$$

where  $\sigma_{URA}^s$  represents the URA parameter of satellite  $s$ .

### B2b GPS clock jump bias and its impact on positioning

As depicted in Fig. 1, B2b clock series are demonstrated and the systematic clock jumps frequently occur simultaneously for all GPS satellites, despite no changes in the

“IOD Corr” parameters during the period. Conversely, the clock corrections for BDS-3 remain consistent until the “IOD Corr” switches. It confirms the presence of systematic jump bias exclusively in the B2b GPS clock.

To delve deeper into the systematic jump, we analyze B2b clock corrections sequence of three days and computed the average jump bias when these jumps occurred. As depicted in Fig. 2, the majority of jump values ranged from  $-2$  to  $1$  m. These jumps exhibited a random occurrence rate of about 8 times per hour, with an average jump bias of 0.61 m.

As illustrated in Fig. 3, the PPP-B2b performance using the BDS/GPS dual-system shows inferior performance compared to BDS-3 only. In this case, the inter-system bias (ISB) parameter is configured as a random walk parameter with a small process noise of  $0.1 \text{ m}/\sqrt{\text{day}}$ . Therefore, GPS clock’s jump bias cannot be absorbed by the ISB parameter thoroughly. The post-test residuals of the dual-system exhibit significant enlargement compared to BDS-3 only, leading to frequent post-test gross error elimination and reinitialization of ambiguity parameters. Even when the process noise is amplified to 1.0, the number of PPP re-convergence occurrences within a single day still reaches three times due to clock bias jumps.

**Fig. 1** BDS-3 (top) and GPS (bottom) clock correction series decoded from BDS B2b frequency. The grey vertical dotted line represents the time of “IOD Corr” change, while the red vertical dotted line denotes the time of systematic clock jump occurs

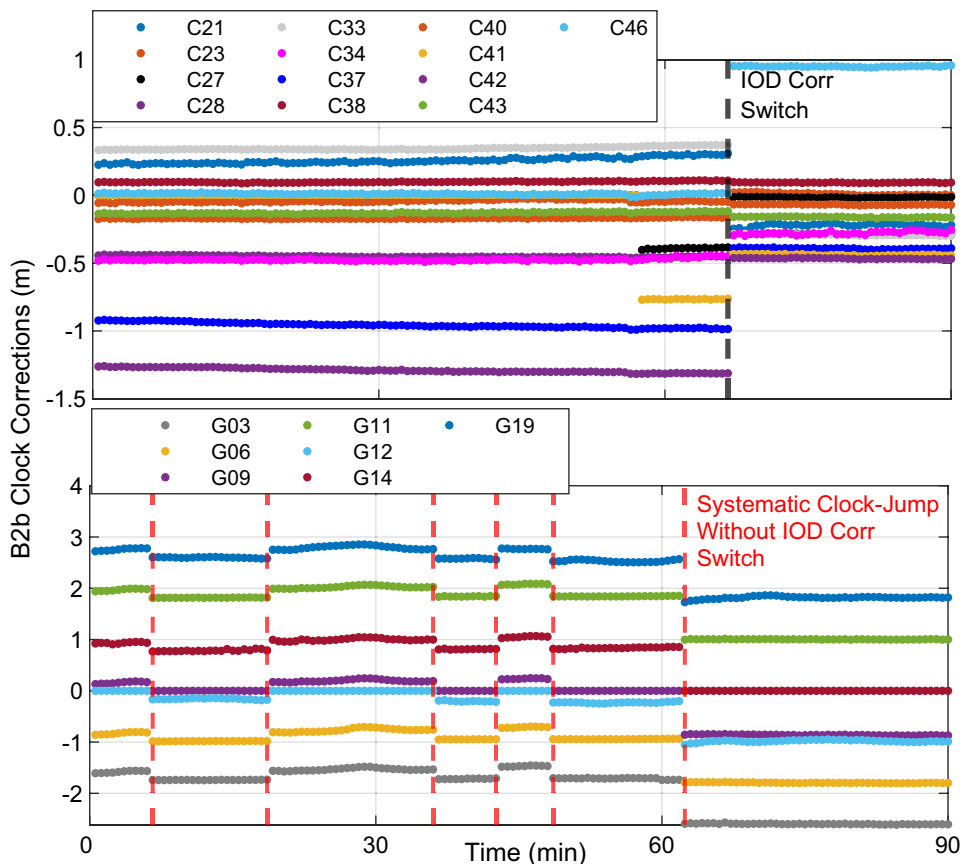


**Fig. 2** B2b GPS clock jump bias statistics in three consecutive days

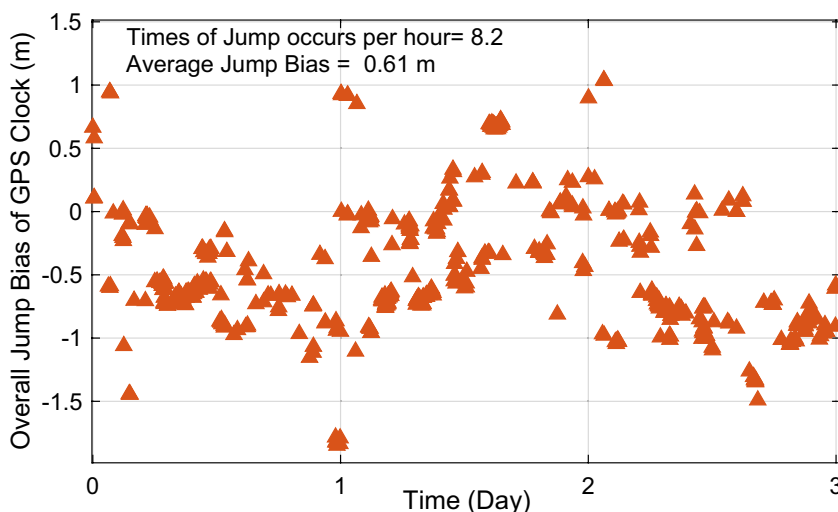
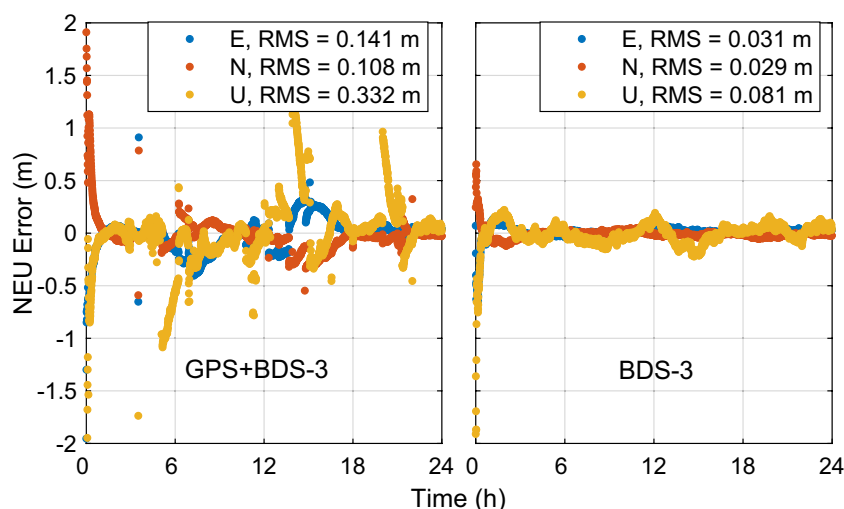


**Fig. 3** Positioning error series using B2b GPS + BDS-3 (left) and BDS-3 only (right). For GPS + BDS-3, ISB is set as random walk parameter and the processing noise is set as 0.1 m/√day



**Strategies to address the GPS clock bias**

Since the jump bias occurs simultaneously for all GPS satellites, it can be detected and corrected to ensure consistency. For GPS B2b products, there is always one satellite with a correction value of zero. When the satellite with the zero value switches, all GPS satellite clock offsets experience a jump simultaneously. Therefore, we monitor the satellite number with the zero value to confirm whether a jump has occurred. In this case, the cause of the jump is likely due to the change of the GPS clock datum. This zero-value satellite is referred to as the reference satellite. When the reference satellite changes, the new reference satellite’s PRN is marked, and the jump bias is calculated by averaging each satellite’s jump value. The specific bias detection and correction process is illustrated in Fig. 4. Figure 5 displays the comparison of clock offset series before and after jump bias detection and correction for GPS satellites. The clock sequence after correction

appears significantly smoother compared to the original one, with the maximum difference reduced to 1.5 m.

Since the jump bias affects all GPS satellites consistently, theoretically, it can be absorbed by the ISB parameter. In this scenario, the ISB would be estimated as white noise (WN) within the extended Kalman filter (EKF) framework (Zumberge et al. 1997), with the parameter in EKF expressed as:

$$\begin{cases} \emptyset_{ISB} = 0 \\ Q_{ISB} = 9 * 10^{10} m^2 \\ P_{0\_ISB} = 9 * 10^{10} m^2 \end{cases} \quad (12)$$

where  $\emptyset_{ISB}$  represents the ISB transition matrix value,  $Q_{ISB}$  denotes the ISB process noise and  $P_{0\_ISB}$  represents the initial variance for ISB parameter.

Besides, the ISB can be estimated as random walk (RW) parameter in EKF as well, which can be expressed as:

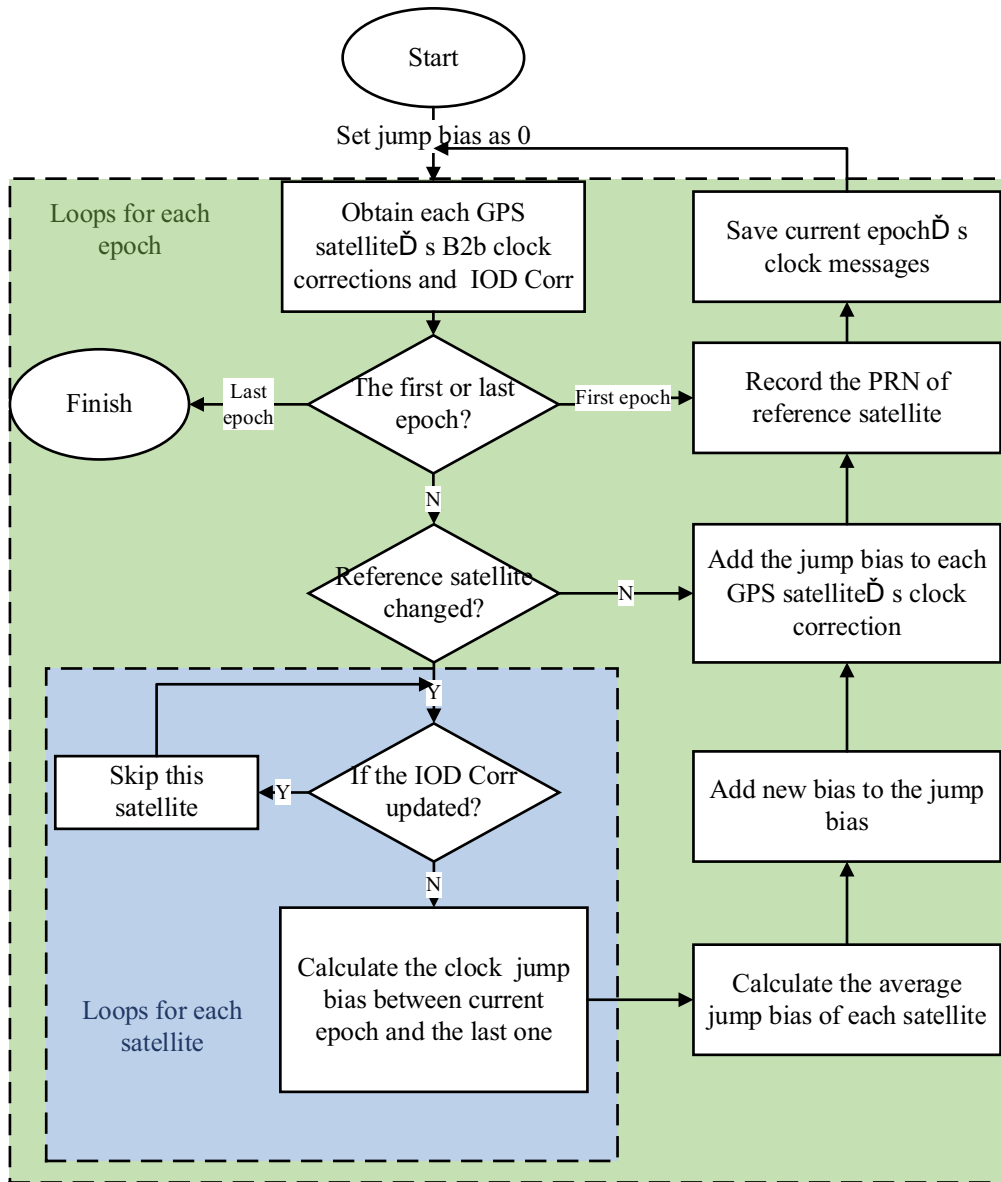


Fig. 4 B2b GPS clock bias jump detecting and splicing strategy

$$\begin{cases} \sigma_{ISB} = 1 \\ Q_{ISB} = Q'^2_{ISB} * \Delta t m^2 \\ P_{0\_ISB} = 1 * 10^2 m^2 \end{cases} \quad (13)$$

where  $Q'_{ISB}$  represents the process noise factor related to time. In this paper, the  $Q'_{ISB}$  varies from 0.1 to 3.0 m/ $\sqrt{\text{day}}$ .

Due to the varying impacts of different ISB estimation strategies on positioning performance (Liu et al. 2022), a detailed analysis of the positioning performance of these strategies will be conducted in the “[Experiments and analysis](#)” section.

### Legacy B2b URA evaluation

The B2b URA series over seven days is depicted in Fig. 6. The URA values for BDS range from 0.02 to 0.20 m, with the majority falling between 0.07 and 0.20 m. Conversely, the URA for GPS is generally larger than that of BDS, with values mostly ranging from 0.22 to 0.67 m.

To validate the performance of the URA-weighting method, we conduct seven days’ PPP using the URA and compare it with the non-URA stochastic model. Note that in this paper, the criteria for determining the PPP convergence

**Fig. 5** GPS satellite (PRN: G19) clock series comparison before (blue) and after (red) bias detection and splicing (top panel). The bottom panel display the difference of two clock time series

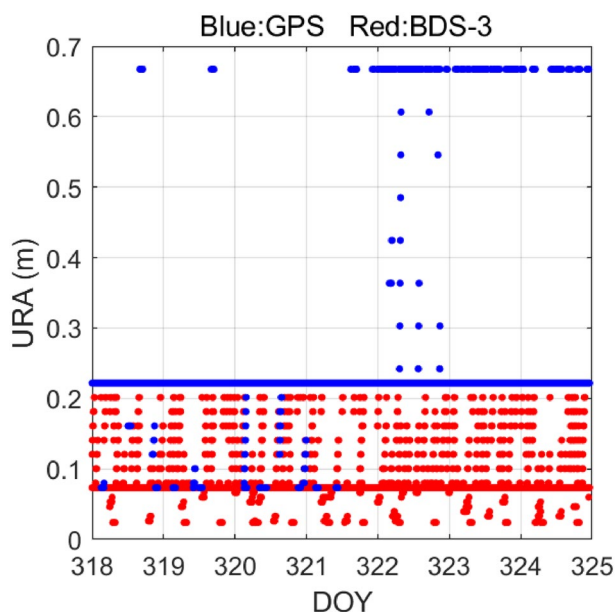
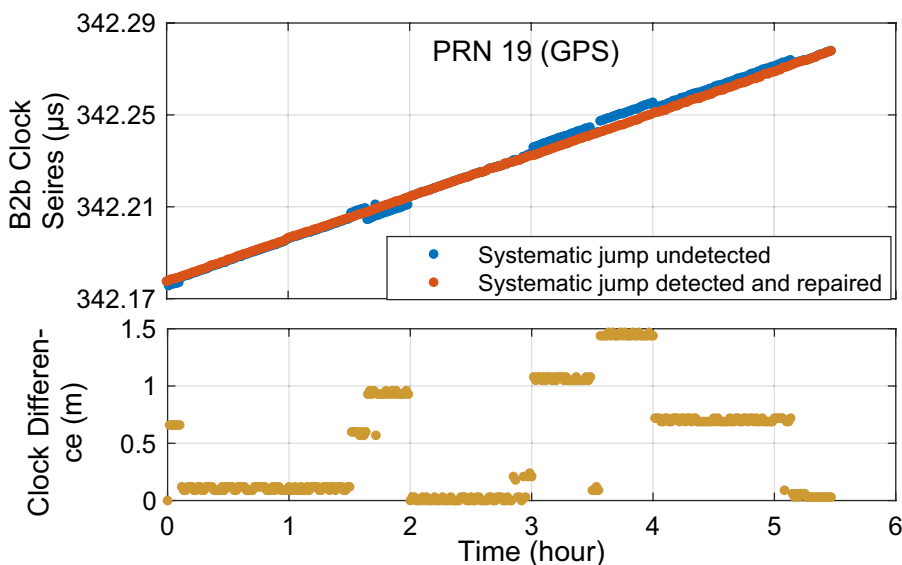


**Fig. 6** The BDS-3 (red) and GPS (blue) URA index time series broadcasted in BDS B2b (year: 2023)

time are as follows: the horizontal errors for ten consecutive epochs must be less than 0.2 m, and the vertical errors must be less than 0.3 m. Besides, RMSE is calculated from the first convergence moment. We employ the bias detection and splicing method to eliminate the GPS clock jump. A one-day positioning resolution comparison is presented in Fig. 7. Compared to the URA-weighting method, the non-URA weighting method exhibits faster convergence time and better accuracy performance. The statistical RMSE and convergence time for both strategies are summarized in Table 2. It's observed that when using PPP-B2b URA, convergence

performance is significantly weakened compared to the non-URA strategy in both kinematic and static modes.

To understand the reason for the weakened performance when using B2b broadcasted URA, further analysis is conducted. As shown in Fig. 6, a large proportion of URA values are larger than 0.1 m, whereas the pseudorange and carrier phase observation noise is typically set as 0.3 m and 0.003 m, respectively. Consequently, the relatively large values of URA in B2b signal significantly reduce the weight of phase observations, which may lead to sharply weakened convergent performance. To utilize URA for weighting while ensuring the weight of phase observation remains appropriate, we propose scaling down the URA at the same epoch with a scale factor  $f_{URA}$ . The updated URA, denoted as  $URA'$ , can be expressed as:

$$URA' = \frac{URA}{f_{URA}} \tag{14}$$

We adjust the URA scale-down factor and re-evaluate the URA-weighted positioning performance. As depicted in Fig. 8, with the increase of the factor, the performance gets closer to the non-URA weighting method without exceeding it. This observation suggests that the precision of the current URA index broadcasted by B2b signals is poor and not suitable for observation weighting, even with the scaling strategy.

### Carrier-phase URA refinement strategy

To address the issue of insufficient accuracy in PPP-B2b broadcasted URA, we propose a refined phase URA re-estimation method. The URA calculation can be expressed as follows:

**Fig. 7** B2b BDS-3 + GPS positioning error time series with URA weighting strategy (left) and non-URA weighting strategy (right). Station: WUH2, day of year (DOY): 318, 2023

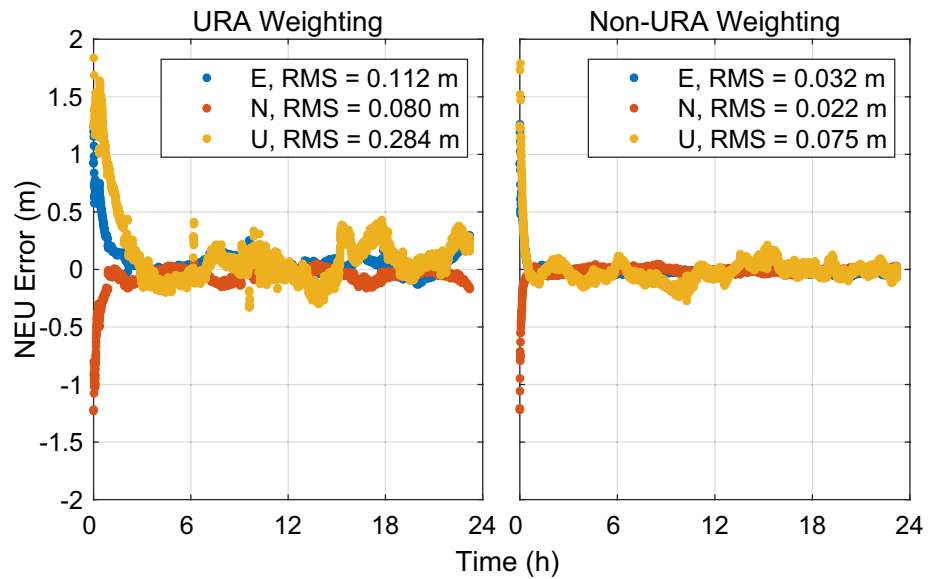


**Table 2** The RMSE and convergence time statistic results for two different strategies (with and without URA in stochastic model)

Mode	Kinematics		Static	
	RMSE (m)	Convergence time (min)	RMSE (m)	Convergence time (min)
With URA	0.20	117.0	0.05	90.0
Non-URA	0.08	20.3	0.04	18.1

$$URA_j^s = \sqrt{\frac{\sum_{i=1}^n \bar{V}_{j,r}^{s2}}{n}} \tag{15}$$

where  $\bar{V}_{j,r}^s$  represents the post residual of satellite  $s$  with phase observation for receiver  $r$  in epoch  $j$ .  $n$  denotes the total station number in the sight of satellite  $s$ .

Figure 9 illustrates the process of real-time BDS-3 phase URA re-estimating based on monitor stations. First, the precise station coordinates need to be calibrated precisely. Then, using the real-time PPP-B2b corrections and observation data from each station, the dual-frequency IF PPP filtering solution with fixed station coordinates can be computed for each epoch. The parameters to be estimated at this stage include the station clock offsets, tropospheric delays, and the IF ambiguities for each satellite. Parameters estimation is performed using Kalman filtering, and the phase residuals are calculated. Theoretically, these phase residuals absorb the projections of orbit and clock errors in the satellite observation direction, as well as phase observation noise. The post-fit residuals are accumulated to establish a sample of 20 epochs of post-fit residuals, thereby improving the reliability of the URA evaluation. Once the sample size meets the requirements, the URA for each satellite is estimated epoch by epoch using a sliding window approach.

The strategy involves two rounds of outlier detection and sample filtering to make quality control in the phase URA calculation. The first round occurs before calculating the URA, focusing on screening the statistical sample: (1) phase residuals are discarded when the satellite elevation angle is less than  $15^\circ$  to avoid contamination from significant phase observation noise or multipath effects; (2)

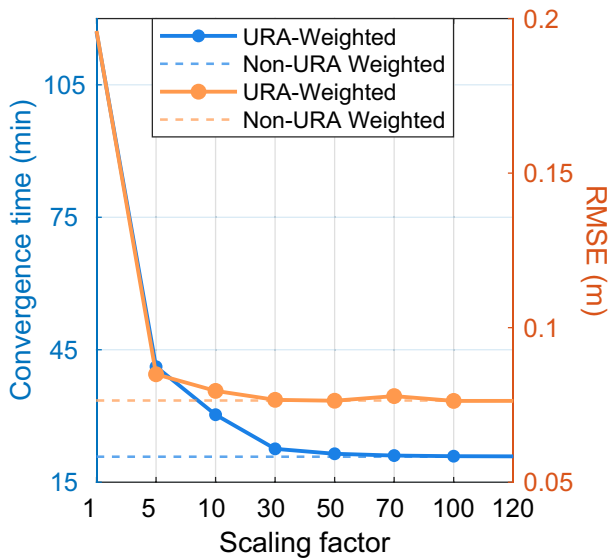
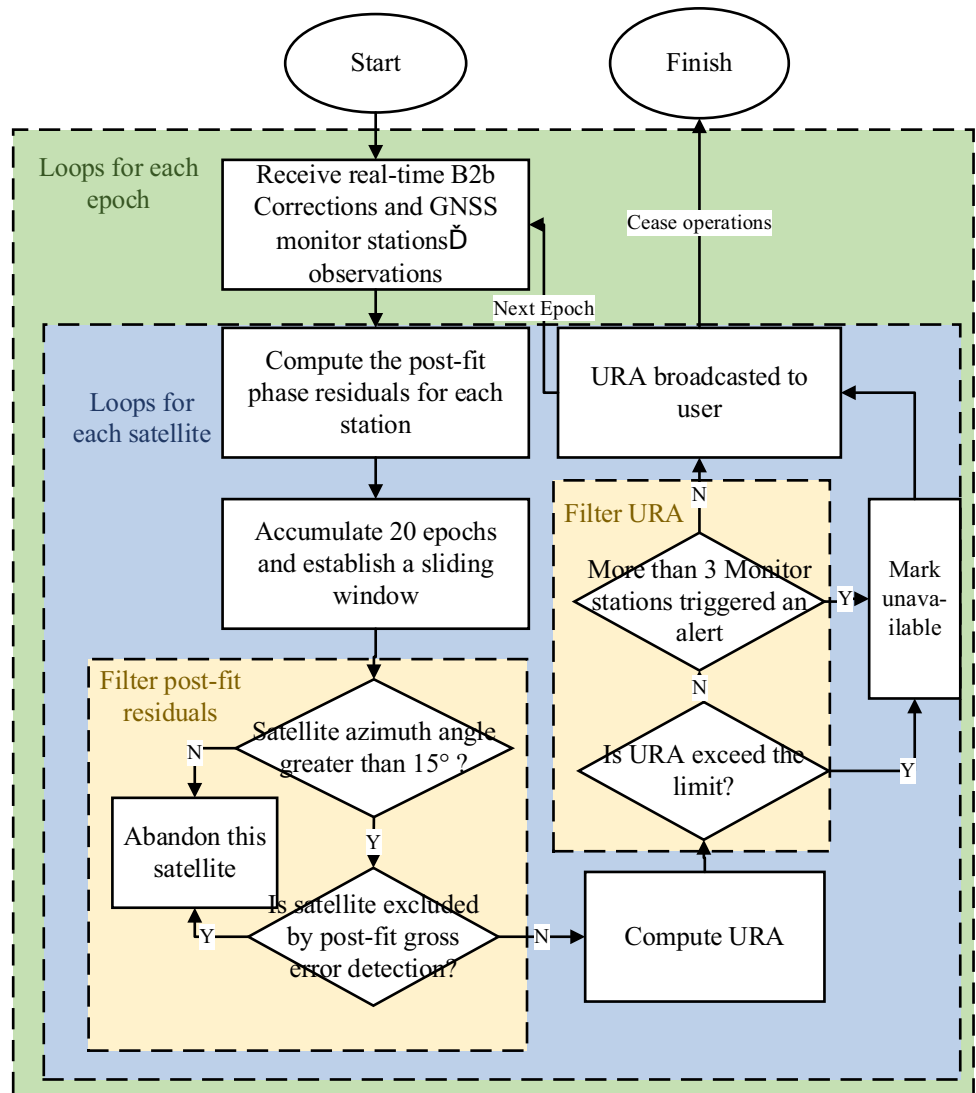


**Fig. 8** URA-weighted PPP performance with different scale down factor

**Fig. 9** Real-time B2b phase URA refinement flowchart



during the real-time filtering and outlier detection process at each monitoring station, any satellites flagged as outliers are excluded from the URA statistical calculations. The second round evaluates the integrity of each satellite after all satellite URAs have been calculated: (1) if more than three monitoring stations consecutively fail the outlier detection for a specific satellite, it is deemed that there are accuracy issues with the satellite’s orbital clock bias, marking it as unusable; (2) any URA values exceeding  $3\sigma$  ( $\leq 99.7\%$ ) are considered outliers, and the corresponding satellite is also marked as unusable. Note that the  $3\sigma$  statistics in the Experiments and analysis section.

Since the refined phase URA incorporates orbital errors, clock bias errors, and the observational noise of phase measurements, the following stochastic model is constructed for phase observations based on this URA:

$$\sigma^s = \sigma_{URA^s} * \varphi = \sigma_{URA^s} * \left( 0.5 + \frac{0.5}{\sin(A_{Ele})} \right) \quad (16)$$

where  $\sigma_{URA^s}$  represents the refined phase URA for satellite  $s$ . Note that the stochastic model for pseudorange observations remains unchanged.

### Experiments and analysis

In this section, experiments are conducted using 7 IGS stations along with 58 stations of China Mobile Shanghai Research Institute (CMSR) distributed in the Asia–Pacific region, shown as Fig. 10. All stations support dual-frequency signals from GPS and BDS-3. Among them, 58 CMSR

**Fig. 10** 7 IGS stations (red) and 58 CMSR stations (blue) distribution

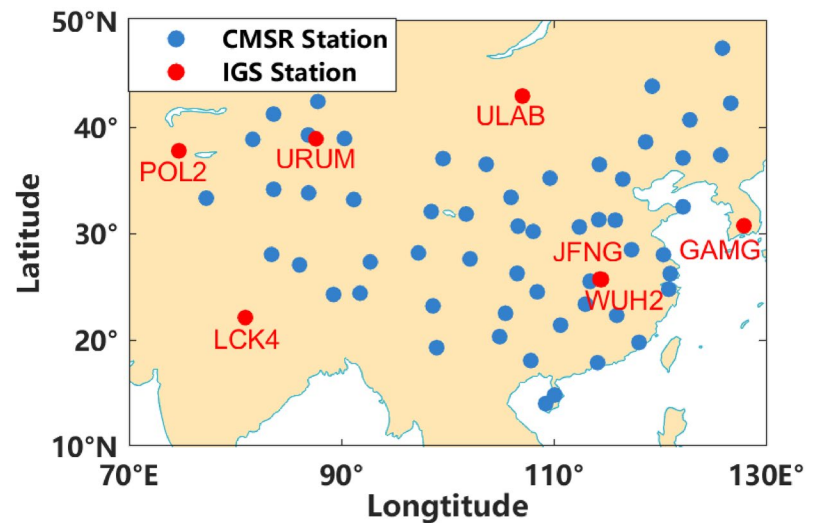


**Table 3** Four strategies to perform PPP-B2b

Strategy no	If use spliced clock	ISB estimation method	Processing noise for ISB
1	Yes	WN	–
2	No	WN	–
3	Yes	RW	0.1–3.0
4	No	RW	0.1–3.0

stations are used for re-estimating the phase URA. Additionally, 7 IGS stations are utilized to analyze the impact of different strategies on positioning performance when handling PPP-B2b clock jumps, and for verifying the positioning performance of the phase URA.

### Comparison of different strategies for B2b GPS clock bias

To evaluate the positioning performance of dual-system PPP-B2b with different strategies, observation data from 7 IGS stations from the day of year (DOY) 318–324 in 2023 are utilized. The true station coordinates are obtained from the solution independent exchange format (SINEX) file provided by IGS, and the daily root-mean-square error (RMSE) is calculated. Both static and kinematic modes are considered, with a sampling interval of 30 s. The Net\_Diff software (Zhang, 2023) is employed for the experiments.

To assess the effectiveness of the spliced GPS clock, dual-system PPP-B2b is conducted using both the spliced clock and the original clock. Beyond that, to explore the impact of different ISB estimation strategies on positioning performance, we estimate the ISB parameters using both methods: white noise estimation and random walk estimation. All four strategies are listed in Table 3.

Figure 11 presents the RMSE and convergence time with four different strategies in both kinematic and static modes. For the white noise estimation strategy, the statistics with clock spliced and non-spliced clocks remain the same, confirming that the jump bias of the GPS clock is systematic and can be fully absorbed by the white noise ISB parameter. In contrast, for the random walk estimation strategy, inappropriate process noise negatively impacts positioning accuracy. Specifically, the three-dimensional error magnifies from 0.08 to 0.832 m in kinematic mode and from 0.035 to 0.037 m in static mode at maximum. Similarly, the convergence time increases from 20.2 to 42.2 min in kinematic mode and from 18.0 to 19.5 min at maximum in static mode. When the process noise is properly set, the performance with RW estimation strategy shows consistency with WN estimation. Note that with the spliced clock and a process noise of 1.0 m/√day, the RW strategy demonstrates optimal positioning performance in kinematic mode.

Moreover, the ideal accuracy is achieved with the clock spliced when setting the process noise to no less than 0.5 m/√day. Conversely, for the original clock without splicing, the process noise needs to be expanded to 2.5 m/√day to counteract the impact of jump bias on dual-frequency positioning. Notably, in the Net\_Diff software, the default setting of process noise in ISB random walk estimation is 1.0 m/√day. In this scenario, the positioning accuracy deteriorates from 0.08 to 0.32 m, while the convergence time improves by 5% for the kinematic mode.

Ultimately, when the systematic bias in the GPS clock is properly handled, errors converge to 0.04 m for horizontal and 0.07 m for vertical with 23 min' convergence time in kinematic mode. In static mode, errors converge to 0.02 m for both horizontal and vertical directions with 18 min' convergence time.

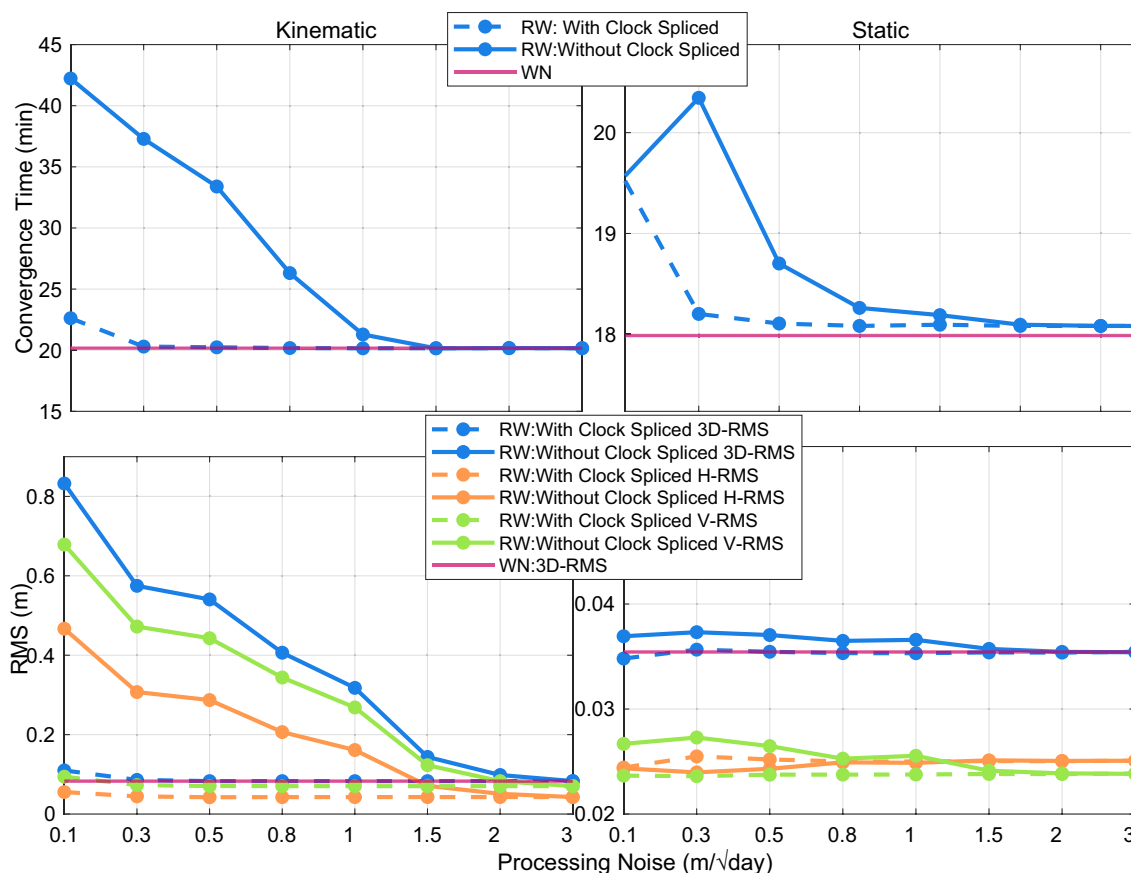


**Fig. 11** B2b GPS + BDS-3 convergence time (top panels) and RMSE (bottom panels) with different ISB processing noise. Both kinematic (left panels) and static (right panels) mode are conducted. The red line represents the statistics with white noise estimation of ISB. The

solid lines indicate the performance without GPS clock bias detected and spliced. The dotted lines indicate the performance using the spliced GPS clock corrections

According to the experiment results, we present three effective strategies for conducting dual system PPP-B2b overall:

- (1) Setting the ISB parameter as white noise. In this case, the ISB parameter can fully absorb the GPS clock jump bias and whether repairing the jump bias of the GPS clock will not affect the positioning performance.
- (2) Setting the ISB parameter as a random walk parameter with a spliced GPS clock. In this case, the process noise of ISB can be set to no less than  $0.5 \text{ m}/\sqrt{\text{day}}$ .
- (3) Setting the ISB parameter as a random walk parameter along with using the original GPS clock without splicing. In this case, the process noise of ISB needs to be larger than  $2.5 \text{ m}/\sqrt{\text{day}}$  to absorb the GPS clock bias.

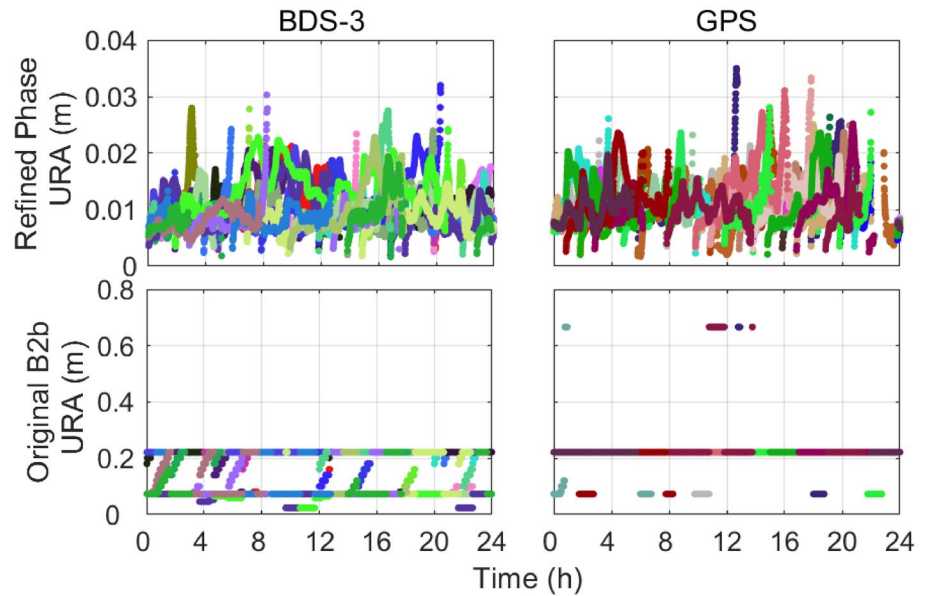
**Refined phase URA and its performance on PPP-B2b positioning**

In this section, all 58 CMSR monitor stations are conducted to re-estimate the phase URA at first. The station coordinate

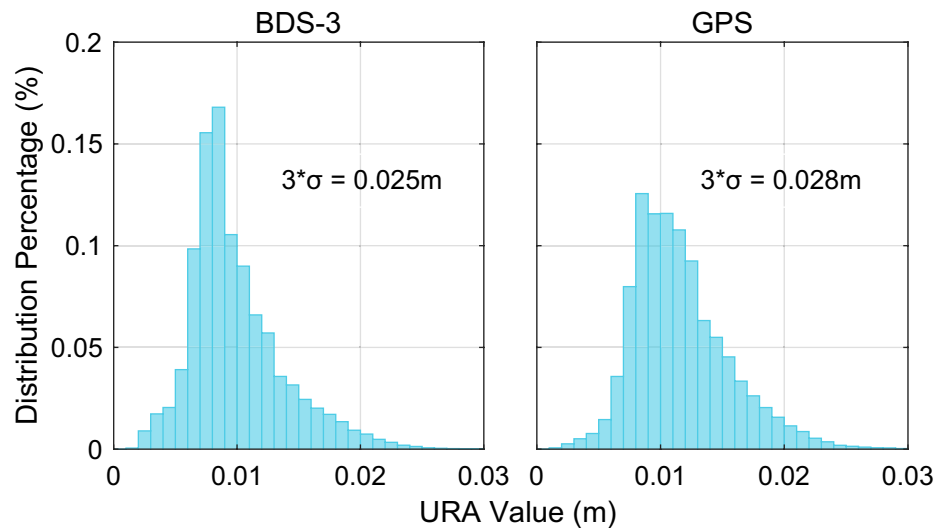
is precisely calibrated using 3 days’ PPP static solutions. Then the stations’ coordinates are fixed to estimate the phase post-residual and statistic the phase URA with the interval of 30 s. Beyond that, to evaluate the refined phase URA, observation data from 7 IGS stations from DOY 003 to 010 in 2024 are utilized. Note that the clock bias of GPS has been properly addressed through clock bias splicing and the implementation of reasonable ISB process noise. Note that to ensure the reliability of the URA this time, we conducted positioning performance validation only after the ambiguity parameters had converged, which can be guaranteed half an hour after the URA calculation began.

Figure 12 shows the optimized estimation of the URA time series for BDS-3 and GPS, along with the original B2b URA over the course of a day. It can be observed that the magnitude of refined phase URA for both systems is much smaller than the broadcasted one. The refined URA for both systems is at the centimeter level, with most values within 3 cm. Further statistical analysis of one week’s refined phase URA distribution range is illustrated in Fig. 13. It can be seen that the URA for BDS-3 satellites is smaller than that

**Fig. 12** Time series of refined phase URA for BDS-3 (top left) and GPS (top right), compared with the origin B2b URA time series calculated by the broadcasted URAI for BDS-3 (bottom left) and GPS (bottom right) (DOY: 001, Year: 2024). Note that different colors are used to distinguish different satellites of the same system



**Fig. 13** Distribution of one week's refined phase URA for BDS-3 (left) and GPS (right)



for GPS, with 99.7% of BDS-3 satellites distributed within 2.5 cm, while 99.7% of GPS satellites are distributed within 2.8 cm. Additionally, the URA for BDS-3 is predominantly between 0.7 and 0.8 cm, whereas the URA for GPS is mainly between 0.8 and 1.1 cm. This distribution reflects that the orbit and clock accuracy of BDS-3 in B2b is slightly better than GPS.

Figure 14 shows the error sequence of single-day solutions for positioning with and without the use of refined URA information. The statistics for the single day indicate that the optimized URA weighting method significantly improves the statistical accuracy of dynamic positioning in the up direction.

The refined phase URA not only enhances the accuracy of the user's positioning but also provides satellite integrity

information through its unusable mark. Figure 15 shows the PPP solution error sequence for JFNG over a specific period. It can be observed that during this period, the refined phase URA issued warnings about satellite unavailability, with the maximum number of unavailable satellites reaching 10, which nearly excluded all BDS-3 satellites. From the positioning error time series and the statistical analysis, it is evident that using the refined phase URA for integrity assessment can effectively ensure positioning stability during periods of satellite anomalies, while users who do not utilize URA information experience prolonged impacts on positioning accuracy after multiple satellite failures.

Considering the impact of monitoring station numbers on real-time data transmission and computational load, as well as the construction and maintenance costs, we further

**Fig. 14** Comparison plot of single-day precise positioning errors with refined phase URA (left) and without URA message (right). Station: WUH2, DOY: 004, 2024

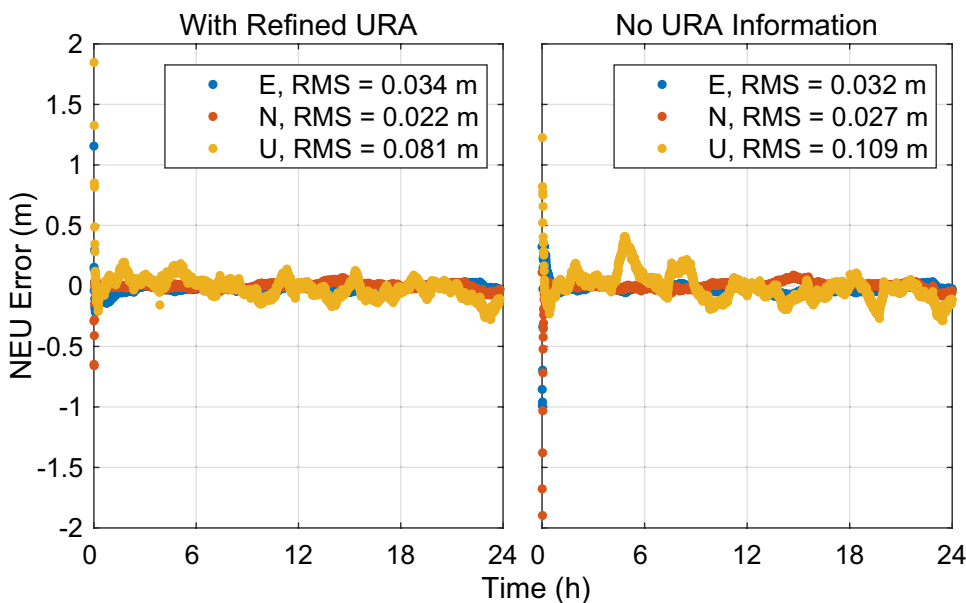
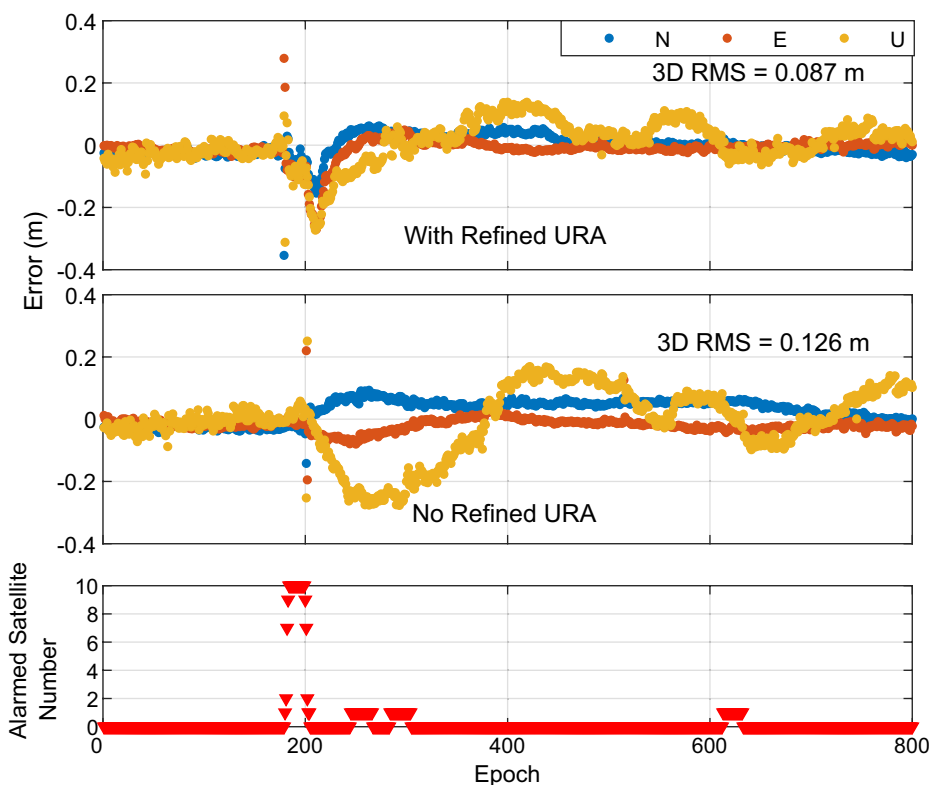


**Fig. 15** The positioning errors series with refined URA (top) and without any URA information (middle), along with the unavailable satellite number (bottom). (Station: JFNG, 2024, DOY: 003)

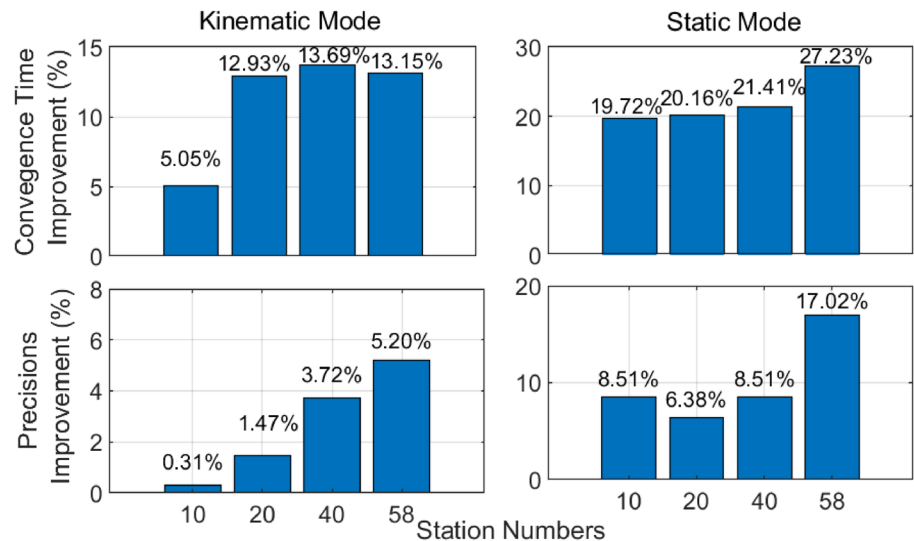


validate how varying the number of stations affects the accuracy of B2b phase URA calculations. We select 10, 20, and 40 stations for refined phase URA estimation and use them to conduct PPP, comparing these results with those obtain from all 58 stations. In these experiments, we ensure that the selected stations are as evenly distributed as possible to maximize the number of visible satellites and minimize the regional correlation of refined URA.

Table 4 shows the statistical results for all stations without URA and with Refined URA computed with different station numbers. The use of refined URA significantly improves the convergence time of B2b-PPP, exceeding 13% for kinematic mode and 27% for static mode. Figure 16 offers a clearer illustration of the percentage improvement in PPP performance resulting from URA estimation with varying station numbers. The figure

**Table 4** Statistical table of PPP-B2b performance with and without refined URA

Mode	Kinematic		Static	
	RMSE (m)	Convergence time (min)	RMSE (m)	Convergence time (min)
Non-URA B2b-PPP	0.129	18.41	0.047	13.59
10 station based Refined-URA B2b-PPP	0.128	17.48	0.043	10.91
20 station based Refined-URA B2b-PPP	0.127	16.03	0.044	10.85
40 station based Refined-URA B2b-PPP	0.124	15.89	0.043	10.68
58 station based Refined-URA B2b-PPP	0.122	15.99	0.039	9.89

**Fig. 16** The improvement of B2b-PPP performance using refined phase URA estimated with different station numbers. The top two subplots in the figure illustrate the convergence time improvement percentage for both kinematic and static modes, respectively. The bottom two subplots in the figure illustrate the precision improvement percentage for both kinematic and static modes, respectively

illustrates that, for the kinematic mode, increasing the number of measurement stations for URA estimation has a limited impact on PPP performance. Despite the number of measurement stations increasing more than fourfold, the enhancement in positioning accuracy is still less than 5%. The enhancement in convergence time is more significant, exceeding 8%. Notably, the figure also indicates that once the number of measurement stations exceeds 20, a boundary effect on convergence time is observed. In contrast, for the static mode, an increase in the number of measurement stations for URA estimation results in a more substantial improvement in both positioning accuracy and convergence time, achieving enhancements of 17% and 27%, respectively. Furthermore, when the number of measurement stations reaches its maximum, there is a marked improvement in static positioning performance. This improvement can be attributed to the enhanced capability of additional measurement stations to detect anomalous satellites, which significantly influence static position calculations, particularly in the initial periods when ambiguities have not been resolved.

## Conclusions

The presence of jump bias in B2b GPS clock and poor accuracy of broadcasted URA parameter deteriorates the accuracy of BDS/GPS dual system PPP-B2b. To mitigate the negative impact of the GPS clock bias, we propose three effective strategies, including a jump bias detection and splicing method combined with different ISB parameter estimation strategies. Three strategies are equivalent in PPP-B2b performance.

With proper handling of the bias, the accuracy of dual-system PPP is significantly improved from 0.83 to 0.08 m, and the convergence time is reduced by up to 22 min in kinematic mode. However, reducing the weight of the GPS system can weaken the negative influence of bias on positioning accuracy, but at the cost of significantly increased convergence time due to less favorable satellite geometry.

Beyond that, we use the URA parameters broadcasted in PPP-B2b signal for constructing the positioning stochastic model, and experimental results reveal its poor accuracy.

Therefore, we propose a refined phase URA estimation strategy along with a matched stochastic model for PPP-B2b. Experiments demonstrate that the refined phase URA significantly improves positioning performance, with 13.2% and 27.2% improvement in convergence time for kinematic and static mode, respectively and with 5.2% and 17.0% improvement in positioning accuracy, respectively. Furthermore, we validate how varying the number of stations affects the accuracy of B2b phase URA calculations. In conclusion, utilizing 20 widely distributed monitoring stations across China satisfies the requirements for URA parameters to enhance real-time kinematic positioning performance. Additionally, increasing the number of measurement stations can further enhance the service performance of URA parameters as an integrity quality indicator to identify anomalous satellites. The work presented in this paper may provide valuable insights for the optimization in the development of BDS-3 PPP-B2b.

**Acknowledgements** The GNSS data provided by China Mobile (Shanghai) Information and Communication Technology Co., Ltd and the IGS Multi-GNSS Experiment (MGEX) network are appreciated. The Real-time SSR corrections from PPP-B2b provided by China BDS-3 official is appreciated. The PPP-B2b message receiving boards provided by ComNav Tech Ltd. is appreciated.

**Author contributions** In this paper, J. C., Z. S. and Y.Z. were responsible for algorithm design. Z. S. and Y. Z. were responsible for the experiments and analysis. J. C and Z. S drafted the paper writing. J. D. optimized the picture format and layout in the paper. X.J., S.Y. and Y. H. are responsible for the observation data collection, preprocessing and quality analysis. All authors have read and agreed to the published version of the manuscript.

**Funding** This research is supported by the National Natural Science Foundation of China (No. 42474034 & No.12403075).

**Data availability** The GNSS data provided by IGS can be achieved through <ftp://gdc.cddis.eosdis.nasa.gov>.

## Declarations

**Competing interests** The authors declare no competing interests.

**Consent for publication** All authors approved the final manuscript and the submission to the journal.

**Ethics approval and consent to participate** Not applicable for the Ethics approval. All authors approved to participate in this work.

## References

- Booth, Janet S., and Robert N. Snow (2009) "An evaluation of OmniStar XP and PPP as a replacement for DGPS in airborne applications." Proceedings of the 22nd International Technical Meeting of the Satellite Division of The Institute of Navigation (ION GNSS 2009), pp. 1188–1194. <https://www.ion.org/publications/abstract.cfm?articleID=8528>
- Chen J, Li H, Wu B, Zhang Y, Wang J, Hu C (2013) Performance of real-time precise point positioning. *Mar Geod* 36(1):98–108. <https://doi.org/10.1080/01490419.2012.699503>
- Chen J, Wang A, Zhang Y, Zhou J, Yu C (2020) BDS satellite-based augmentation service correction parameters and performance assessment. *Remote Sens* 12(5):766. <https://doi.org/10.3390/rs12050766>
- Chen J, Wang J, Yu C, Zhang Y, Wang B (2022a) Improving BDS broadcast ephemeris accuracy using ground-satellite-link observations. *Satell Navig* 3(1):11. <https://doi.org/10.1186/s43020-022-00072-4>
- Chen J, Zhang Y, Yu C, Wang A, Song Z, Zhou J (2022b) Models and performance of SBAS and PPP of BDS. *Satell Navig* 3(1):4. <https://doi.org/10.1186/s43020-022-00065-3>
- CSNO, Chinese Satellite Navigation Office, BeiDou navigation satellite system signal in space interface control document open service signal B2b (Version 1.0), 2020.
- Dai L, Chen Y, Lie A, Zeitzev M, Zhang Y (2016) StarFire™ SF3: worldwide centimeter-accurate real time GNSS positioning. In Proceedings of the 29th International Technical Meeting of the Satellite Division of The Institute of Navigation (ION GNSS+2016) (pp. 3295–3320). <https://doi.org/10.33012/2016.14673>
- European GNSS Service Centre (2023). Galileo high accuracy service service definition document (HAS SDD) (Issue 1.0). [https://www.gsc-europa.eu/sites/default/files/sites/all/files/GalileoHAS-SDD\\_v1.0.pdf](https://www.gsc-europa.eu/sites/default/files/sites/all/files/GalileoHAS-SDD_v1.0.pdf)
- Fernandez-Hernandez I, Chamorro-Moreno A, Cancela-Diaz S, Calle-Calle JD, Zoccarato P, Blonski D et al (2022) Galileo high accuracy service: initial definition and performance. *GPS Solut* 26(3):65. <https://doi.org/10.1007/s10291-022-01247-x>
- Geng J, Zhang H, Li G, Aoki Y (2024) Multipath mitigation for GPS/Galileo/BDS-3 precise point positioning with overlap-frequency signals. *Satell Navig* 5(1):22. <https://doi.org/10.1186/s43020-024-00144-7>
- He Q, Chen L, Liu L, Zhao D, Gong X, Lou Y, Guan Q (2023) Long-term performance evaluation of BeiDou PPP-B2b products and its application in time service. *Remote Sens* 15(5):1358. <https://doi.org/10.3390/rs15051358>
- IGS (2020) IGS state space representation (SSR) format version 1.00. RTCM SC-104 SSR Working Group and IGS Real-Time Working Group, Arlington, TX, USA. Available on: <https://files.igs.org/pub/data/format/>.
- Kouba J, Héroux P (2001) Precise point positioning using IGS orbit and clock products. *GPS Solut* 5:12–28. <https://doi.org/10.1007/PL00012883>
- Leandro R, Landau H, Nitschke M, Glocker M, Seeger S, Chen X, et al (2011) RTX positioning: the next generation of cm-accurate real-time GNSS positioning. In Proceedings of the 24th International technical Meeting of the Satellite Division of the Institute of Navigation (ION GNSS 2011) (pp. 1460–1475). <https://www.ion.org/publications/abstract.cfm?articleID=9705>
- Liu X, Jiang W, Li P, Deng Z, Ge M, Schuh H (2023) An extended inter-system biases model for multi-GNSS precise point positioning. *Meas* 206:112306. <https://doi.org/10.1016/j.measurement.2022.112306>
- Malys S, Jensen PA (1900) Geodetic point positioning with GPS carrier beat phase data from the CASA UNO experiment. *Geophys Res Lett* 17(5):651–654. <https://doi.org/10.1029/GL017i005p00651>
- Odiijk D, Zhang B, Khodabandeh A, Odolinski R, Teunissen PJ (2016) On the estimability of parameters in undifferenced, uncombined GNSS network and PPP-RTK user models by means of S-system theory. *J Geod* 90(1):15–44. <https://doi.org/10.1007/s00190-015-0854-9>
- RTCM Special Committee (2016) RTCM Standard 10403.3 differential GNSS (Global Navigation Satellite Systems) services-version 3. RTCM Special Committee No. 104, Arlington, TX, USA.

- Shi J, Yuan X, Cai Y, Wang G (2017) GPS real-time precise point positioning for aerial triangulation. *GPS Solut* 21:405–414. <https://doi.org/10.1007/s10291-016-0532-2>
- Song Z, Chen J, Zhang Y, Yu C, Ding J (2023) Real-time multi-GNSS precise point positioning with ambiguity resolution based on the BDS-3 global short-message communication function. *GPS Solut* 27(3):136
- Sun S, Wang M, Liu C, Meng X, Ji R (2023) Long-term performance analysis of BDS-3 precise point positioning (PPP-B2b) service. *GPS Solut* 27(2):69. <https://doi.org/10.1007/s10291-023-01409-5>
- Tao J, Liu J, Hu Z, Zhao Q, Chen G, Ju B (2021) Initial assessment of the BDS-3 PPP-B2b RTS compared with the CNES RTS. *GPS Solut* 25:1–6. <https://doi.org/10.1007/s10291-021-01168-1>
- Cabinet Office, Government of Japan (2022) Trial service of MADOCA-PPP has now started [EB/OL]. [https://qzss.go.jp/en/overview/notices/madoca\\_220930.html](https://qzss.go.jp/en/overview/notices/madoca_220930.html).
- Wang A, Chen J, Zhang Y, Wang J, Wang B (2020) BDS/GPS combined kinematic precise point positioning based on zone corrections. *J Tongji Univ* 48(3):447–455
- Wang A, Zhang Y, Chen J, Wang H (2022) Improving the (re-)convergence of multi-GNSS real-time precise point positioning through regional between-satellite single-differenced ionospheric augmentation. *GPS Solut* 26(2):26–39. <https://doi.org/10.1007/s10291-022-01229-z>
- Wang Y, Li R (2013) The analysis of character of user range accuracy. In *China Satellite Navigation Conference (CSNC) 2013 Proceedings: Satellite Navigation Signal System, Compatibility & Interoperability Augmentation & Integrity Monitoring Models & Methods* (pp. 267–277). Springer Berlin Heidelberg. [https://doi.org/10.1007/978-3-642-37404-3\\_24](https://doi.org/10.1007/978-3-642-37404-3_24)
- Wang J, Li Q, Liu R (2019) Improvement of positioning accuracy with GNSS using user range accuracy and posterior variance model. In *Proceedings of the 32nd International Technical Meeting of the Satellite Division of The Institute of Navigation (ION GNSS+ 2019)* (pp. 1488–1495). <https://doi.org/10.33012/2019.16910>
- Weber G, Mervart L, Lukes Z, Rocken C, Dousa J (2007) Real-time clock and orbit corrections for improved point positioning via NTRIP. In *Proceedings of the 20th international technical meeting of the satellite division of the institute of navigation (ION GNSS 2007)* (pp. 1992–1998). <https://www.ion.org/publications/abstract.cfm?articleID=7413>
- Wu P, Lou Y, Zhang W, Dousa J, He H, Chai J et al (2023) Evaluation of real-time kinematic positioning performance of the BDS-3 PPP service on B2b signal. *GPS Solut* 27(4):192. <https://doi.org/10.1007/s10291-023-01532-3>
- Xu Y, Yang Y, Li J (2021) Performance evaluation of BDS-3 PPP-B2b precise point positioning service. *GPS Solut* 25(4):142. <https://doi.org/10.1007/s10291-021-01175-2>
- Xu X, Nie Z, Wang Z, Zhang Y, Dong L (2023) An improved BDS-3 PPP-B2b positioning approach by estimating signal in space range errors. *GPS Solut* 27(3):110. <https://doi.org/10.1007/s10291-023-01455-z>
- Zhang Y. (2023) The open accessed software is available on [https://github.com/YizeZhang/Net\\_Diff](https://github.com/YizeZhang/Net_Diff).
- Zhang Y, Nobuaki K, Chen J, Wang J, Wang H (2019) Initial positioning assessment of bds new satellites and new signals. *Remote Sens* 11(11):1320. <https://doi.org/10.3390/rs11111320>
- Zumberge JF, Heflin MB, Jefferson DC, Watkins MM, Webb FH (1997) Precise point positioning for the efficient and robust

analysis of GPS data from large networks. *J Geophys Res Solid Earth* 102(B3):5005–5017. <https://doi.org/10.1029/96JB03860>

**Publisher's Note** Springer Nature remains neutral with regard to jurisdictional claims in published maps and institutional affiliations.

Springer Nature or its licensor (e.g. a society or other partner) holds exclusive rights to this article under a publishing agreement with the author(s) or other rightsholder(s); author self-archiving of the accepted manuscript version of this article is solely governed by the terms of such publishing agreement and applicable law.



**Junjing Chen** is a professor and the head of the GNSS data analysis group at Shanghai Astronomical Observatory (SHAO). He received his Ph.D. degree in Satellite Geodesy from Tongji University in 2007. He is the president of the International Association of Chinese Professionals in Global Navigation Satellite Systems (CPGNSS). His research interests include multi-GNSS data analysis and GNSS augmentation systems.



**Ziyuan Song** is currently an Algorithm Engineer in the Spatiotemporal Information Products Department at China Mobile (Shanghai) Information and Communication Technology Co., Ltd. He received his Ph.D. degree in Shanghai Astronomical Observatory (SHAO), Chinese Academy of Sciences in 2024. His current research mainly focuses on Multi-GNSS PPP-RTK integrity resolution.



**Yize Zhang** is currently an associate professor at Shanghai Astronomical Observatory (SHAO). He received his Ph.D. degree from Tongji University in 2017. Then, he did his postdoctoral research at the Tokyo University of Marine Science and Technology (TUMSAT). His current research mainly focuses on multi-GNSS precise positioning and GNSS biases analysis.



**Junsheng Ding** is currently a postdoctoral fellow at the Department of Land Surveying and Geo-Informatics, the Hong Kong Polytechnic University (PolyU). He obtained his bachelor's degree in 2018 from Chang'an University, China, and his Ph.D. degree in 2023 from the Shanghai Astronomical Observatory, Chinese Academy of Sciences and School of Astronomy and Space Science, University of Chinese Academy of Sciences. His current research interests include GNSS Meteor-

ology and AI for Geodesy.



**Xin Jiang** is a professor-level senior engineer, currently serves as the General Manager of the Spatiotemporal Information Products Department at China Mobile (Shanghai) Information and Communication Technology Co., Ltd. His primary research focuses on precision positioning using 5G and GNSS technology.



**Sainan Yang** Ph.D., currently serves as an Algorithm Engineer in the Spatiotemporal Information Products Department at China Mobile (Shanghai) Information and Communication Technology Co., Ltd. Her main research focuses on precision positioning using 5G and GNSS technology.



**Yangfei Hou** is currently a postdoctoral researcher at China Mobile (Shanghai) Information and Communication Technology Co., Ltd. He received his Ph.D. degree from Tongji University in 2023. His current research mainly focuses on GNSS real-time precise point positioning.